Ultraviolet micro-Raman stress map of polycrystalline diamond grown selectively on silicon substrates using chemical vapor deposition

Raju Ahmed,[1] M. Nazari,[1] B. L. Hancock,[1] J. Simpson,[1] C. Engdahl,[2] E. L. Piner,[1,3] and M. W. Holtz[1,3]
[1]*Materials Science, Engineering, and Commercialization, Texas State University, San Marcos, Texas 78666, USA*
[2]*Crystallume, Inc., 3397 De La Cruz Boulevard, Santa Clara, California 95054, USA*
[3]*Department of Physics, Texas State University, San Marcos, Texas 78666, USA*

(Received 2 March 2018; accepted 17 April 2018; published online 3 May 2018)

Polycrystalline diamond stripes, with a nominal thickness of ∼1.5 μm and various widths, were selectively grown on silicon substrates using chemical vapor deposition. Stress measurements using ultraviolet micro-Raman mapping reveal high compressive stress, up to ∼0.85 GPa, at the center of the diamond stripe, and moderate tensile stress, up to ∼0.14 GPa, in the substrate close to the interface with the diamond. Compressive stresses on diamond decrease with diminishing stripe widths. The stress map is well-described using finite element simulation incorporating solely thermal expansion effects. *Published by AIP Publishing*. https://doi.org/10.1063/1.5027507

Thermal management in electronics is the principal limiting factor to increasing power while reducing size and increasing density of devices. The high thermal conductivity of diamond has motivated efforts for integration with various electronic materials for passive reduction of local heating in devices.[1,2] Polycrystalline diamond, which can be grown on diverse substrates using chemical vapor deposition (CVD), is a prospective heat spreading layer due to improvements reported in thermal performance of power transistors.[3,4] However, the 700–800 °C growth temperature used for hot-filament (HF) CVD diamond and the large difference in the coefficient of thermal expansion (CTE) between diamond and the substrate produce thermal stresses in both materials.[5,6] In addition to thermal stresses, the diamond CVD process may produce intrinsic stresses which can have significant deleterious effects on the overall mechanical properties of the diamond and substrate. Stress can affect device performance, through changes in the electronic properties, and lead to failure, while excessive stresses on the substrate may bow and even shatter the wafer.[7]

Wafer stress, due to uniform diamond layer deposition, may be mitigated by producing a patterned diamond structure. Although patterned diamond will not eliminate *local* stresses associated with layer coverage, the presence of open regions permits relaxation of the *global* substrate stress. One approach for producing a patterned diamond layer is blanket CVD coverage of the substrate followed by etch removal of selected regions.[8] This "top-down" method does not, however, eliminate the uniform thermal stress produced by the initial diamond layer deposition. Furthermore, complete removal of the diamond from the substrate is difficult and prospectively destructive to the etch fields.[8] An alternative approach, used here, is based on a "bottom-up" procedure in which diamond is only seeded in desired regions[9] of a substrate, such as silicon. Subsequent CVD growth takes place only in the seeded areas. We find that this method results in high selectivity and relaxes global stress. Regions covered by diamond, and the silicon substrate itself, are under local mechanical stress as revealed using ultraviolet (UV) micro-Raman mapping.

Selective deposition of CVD diamond stripes on 100-mm Si (001) wafers began by patterning the wafer with nano-diamond seeds, which are ubiquitous for initiating growth. Dimethyl sulfoxide based nano-diamond suspension (Adamas Nanotech., 0.5 wt. % nano diamond seeds, ∼4 nm average diameter, 20–30 nm aggregate size) was dispersed in photoresist (Shipley 1813). Approximately 5 ml of the solution was sonicated, spun on the wafer, and soft baked at 110 °C for 90 s, followed by exposure using contact photolithography (SUSS MicroTec). Developing produced regions of seed-laden resist surrounded by cleared silicon fields. To improve selectivity, the wafer is subjected to plasma processing (dual-power reactive-ion etching and inductively coupled plasma at 150 and 1500 W, respectively) in 45 sccm CF_4 and 5 sccm O_2. This etch helped remove seeds remaining in the opened fields. The resist-patterned wafer was loaded into a hot filament CVD chamber (Crystallume, Inc.). A 1.5% mixture of methane (30 sccm) and hydrogen (2 l/min) was used for diamond growth, with substrate temperature in the range of 720–750 °C. The resulting diamond was characterized using scanning electron microscopy (SEM, FEI Helios 400), atomic force microscopy (AFM, Bruker Dimension ICON), and surface profilometry (DektakXT). Good across-wafer uniformity was achieved in diamond growth. Effects due to microloading were not observed.

Figure 1(a) shows a representative optical image from the processed wafer. The nominally 20-μm wide diamond stripes and bare Si fields are clearly defined. The SEM image in Fig. 1(b) is from a representative stripe, as depicted by the circle in Fig. 1(a). Several micron-scale diamonds are observed in the Si fields in the SEM image; these may be a result of nano-diamonds which either remain following the seeding process or which redeposit during the initial diamond growth stage. The unwanted seeding density depends on the resist removal efficacy, thereby supporting the former interpretation but without ruling out the latter. Stripes are

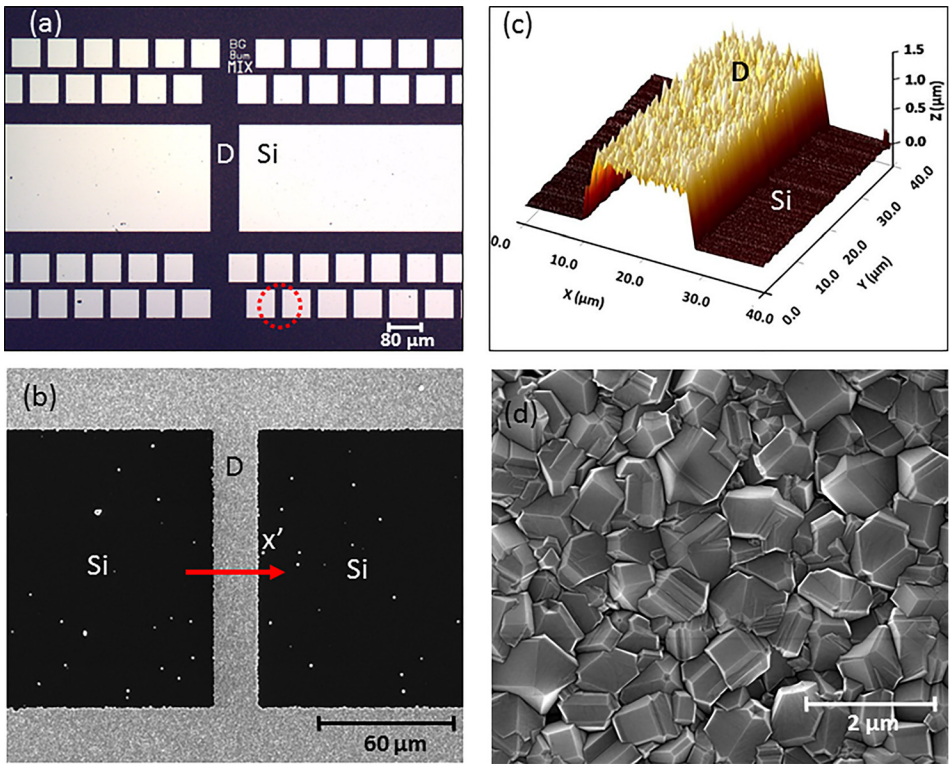

FIG. 1. (a) Optical image of selectively grown diamond taken from a region with various size stripes and windows; (b) SEM image exhibiting a 20-μm wide diamond stripe and silicon fields; (c) AFM image of a 20-μm wide diamond stripe; and (d) Close-up SEM image of the diamond-covered surface.

perpendicular to the (110)-oriented flat on the Si wafer so that micro-Raman images, described below, are along a $\langle 110 \rangle$ direction that we denote x'. In Fig. 1(c), we show an AFM image of a representative 20-μm wide stripe. From AFM images, we determine the nominal thickness of 1.5 μm, and from 10-μm × 10-μm scan areas (not shown), the root-mean squared (RMS) roughness of the diamond is determined to be ∼80 nm. The micron-scale polycrystals achieved under these growth conditions are shown in Fig. 1(d) from a close-up plan-view SEM image.

Micro-Raman spectroscopy is powerful for assessing diamond material quality and for measuring mechanical stress.[10] Extensive research has been conducted on stress measurements of CVD diamond[11] and Si[12] based on Raman spectroscopy. Here, we employ UV micro-Raman imaging, with an excitation wavelength of 363.8 nm, for two reasons. First, low fluorescence background from diamond allows observation of sharp O(Γ)-symmetry phonons in silicon (520 cm^{-1}) and diamond (1332 cm^{-1}) and the broad non-diamond carbon (NDC) spectrum (1450–1600 cm^{-1}).[13] Second, the shallow probe depth at this wavelength in Si permits the study of the topmost ∼5-nm,[14] where stress is expected to be most significant. An imaging line focus[15] was implemented to simultaneously map stress along the full lateral width of the diamond stripe in a single acquisition. Spectra collected in this mode generate a 400 × 1340-pixel image using a charge-coupled device detector. The image spans the stripe x' direction with the Raman spectra dispersed in the longer detector dimension. This extensively simplifies performing line maps and obviates laser heating since the power density at the sample surface is $<10\,\mu\text{W}/\mu\text{m}^2$. Full accumulation required an acquisition time of 1 to 10 min.

Figure 2 shows a typical Raman spectrum (polarization not analyzed) extracted from the line image corresponding to the center of the 20-μm wide diamond stripe. Clearly seen are the silicon and diamond phonons and the broad Raman scatter from NDC. The O(Γ)-symmetry phonons are each fit using a single Lorentzian line shape. Line widths near the stripe centers are ∼6.4 cm^{-1} for silicon and ∼8.2 cm^{-1} for diamond without correcting for the instrumental response. The setup permits observation of shifts ≤ 0.1 cm^{-1} with a peak position uncertainty of 0.02 cm^{-1} based on fits. For uniform layer coverage, the Raman shift may be used to estimate biaxial stress via

$$\sigma_B = -k_R(\omega - \omega_o) = -k_R \Delta\omega, \tag{1}$$

where k_R is the Raman stress factor for either silicon or diamond and $\Delta\omega$ is frequency shift from the corresponding strain-relaxed material. A red shift corresponds to tensile stress ($\sigma_B > 0$), while a blue shift corresponds to compressive

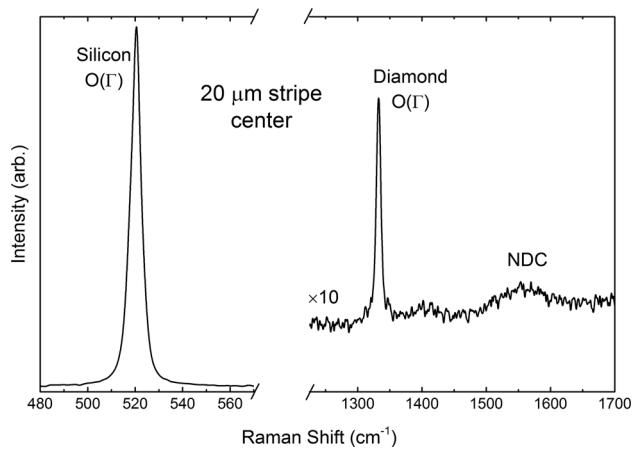

FIG. 2. Raman spectrum obtained from the line image at the center of the 20-μm wide diamond stripe.

stress ($\sigma_B < 0$). Values for ω_0 were obtained prior to each measurement using bulk silicon and natural diamond reference samples.

Mapping transverse to the diamond stripe produces a stress map of the silicon and diamond, as presented in Fig. 3 across representative widths of 20, 40, and 80 μm. The left- and right-hand series of panels are for silicon and diamond, respectively. Note that the scales are different for each panel series. Raw data for $\Delta\omega$ versus position are shown as points. Individual values correspond to an average of five detector pixels, corresponding to a distance of $\sim$2.3 μm, which is close to the measured microscope resolution. A systematic variation in stress is observed in each panel. For the diamond, the maximum shift (compressive stress) occurs near the center of each stripe. Stress diminishes close to the edges due to the free sidewalls which permit relaxation through less constrained expansion. The smaller shifts observed in Si beneath the diamond correspond to a lower tensile stress. Close to the edge of each stripe, an enhancement of the shift (stress) in silicon is observed due to edge discontinuity. Separate measurements confirm that stress in silicon relaxes far from the diamond stripes.

Thermal stresses due to cooling from the CVD growth temperature were simulated using a two-dimensional (2D) finite element (FE) analysis. To calculate thermal stresses, temperature-dependent CTEs were employed using data published for silicon[16] and diamond.[17] Other material parameters for CVD diamond are taken from Hess[18] and elastic moduli for Si are taken from Hopcroft *et al.*[19] The simulated thermal stress $\sigma_{x'x'}$ is representative of the lateral dependence expected within the diamond and silicon due to the selective growth and is found to compare well with our Raman maps.

Figure 4 shows a representative 2D simulation of in-plane stress perpendicular to the stripe and near its edge. Diamond stress is enhanced near the edge of the stripe close to the interface with silicon but relaxes in the unconstrained corner region of the diamond. The lateral (x') extent of the relaxed diamond corner is several times the 1.5-μm thickness, as expected for a "hard" stripe on a "soft" substrate.[20] Far from the diamond, the stress is relaxed in silicon. The stress in the diamond exhibits better uniformity at distances far from the stripe edge. Stress is present in the silicon

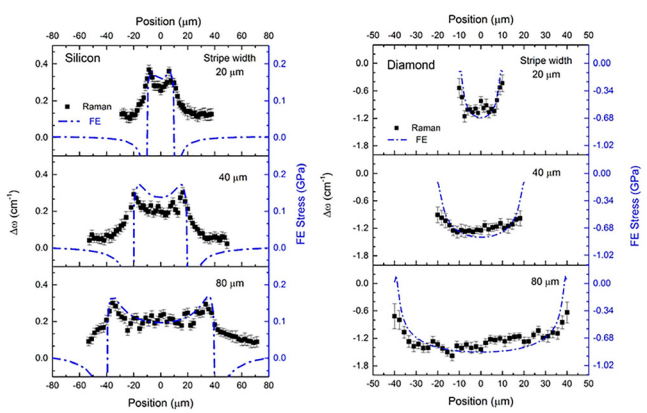

FIG. 3. Raman measurement (points) and FE simulation stress maps (curves) of the silicon (left) and diamond (right) as a function of position across three representative stripe widths: 20, 40, and 80 μm.

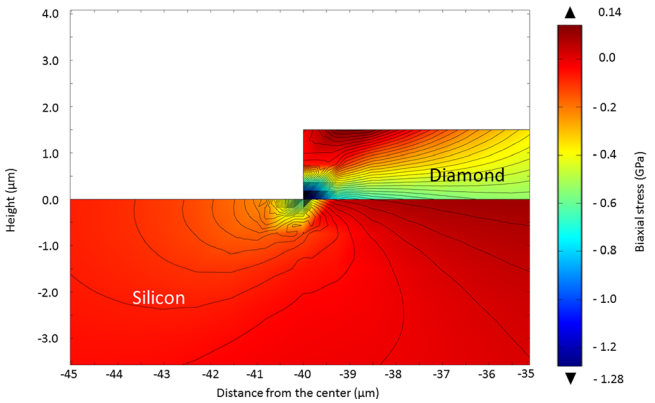

FIG. 4. Close-up 2D stress simulation near the edge of an 80-μm wide and 1.5 μm thick diamond stripe grown on a 500-μm thick Si substrate.

immediately beneath the diamond and relaxes by a factor of $\sim$1/3 at a depth of 5 μm (not shown).

To compare computed stress with our measurements, we examine horizontal cut lines at select depths following the simulation. For the transparent diamond, we average the results of cut lines from five depths throughout the diamond. In silicon, optical attenuation weights the observed stress according to

$$\langle \sigma_{x'x'}(Si) \rangle = \frac{\int_0^\infty \sigma_{x'x'}(z) e^{-z/d_{OPT}} dz}{\int_0^\infty e^{-z/d_{OPT}} dz}, \tag{2}$$

where $z = 0$ corresponds to the interface, $z > 0$ is the depth within the silicon, and $d_{OPT} = 1/(\alpha_L + \alpha_S) \approx 5$ nm is the effective optical penetration depth. Published absorption coefficients $\alpha_{L(S)}$ are taken at the laser (L) and scattered (S) wavelengths.[21] To approximate Eq. (2), we extract cut lines at ten z values spaced 1 nm apart and compute the weighted average. For diamond and silicon, we perform a horizontal boxcar average corresponding to the $\sim$2-μm microscope resolution. The averaging has the benefit of reducing the impact of mesh-related effects in the FE method.

Returning to Fig. 3, the simulated stresses are shown as dotted-dashed curves. Scaling of the shift in Raman position with stress is accomplished by direct application of Eq. (1) and published stress factors $k_R = 0.434$ GPa/cm^{-1} for Si[12] and 0.57 GPa/cm^{-1} for diamond.[8] The good overall agreement confirms the stress in our diamond stripes to be primarily thermal in origin. The Raman-stress estimate obtained using Eq. (1) is not improved when we apply the more detailed analysis of Refs. 22 and 23. We therefore restrict ourselves to the simple approach. For diamond, stress toward the center of each stripe is the greatest and decreases with the narrower stripe width. This is phenomenologically due to the greater relative factor of available free-surface sidewalls for strain relaxation. There is also an $\sim$0.1 GPa discrepancy between simulation and data toward the stripe centers which may be due to slight relaxation into available free volume within the polycrystalline diamond. It is also seen from Fig. 3 that the tensile stress in Si increases as the width of the stripes decreases due to the influence of both edges of the diamond stripe which concentrate the tensile

stress in the substrate. This concentration of stress increases for the smaller stripe width. Our measurements did not reveal the simulated compressive stress spikes present in the silicon beneath the stripe edges. This compression compensates for the stress which would otherwise be provided by the diamond in a uniform layer. A possible interpretation of this discrepancy is the relatively ragged diamond stripe edges, which will blur stress dependences and even mix stress components due to the local normal to the stripes. To check this interpretation, a 3D FE model was produced incorporating a simple zigzag edge for the diamond stripe. We average stress in the silicon using a lateral window and Eq. (2) vertically, as described for the sharp diamond stripe simulations. Stress in the diamond and that in silicon beneath the stripe are not significantly affected when simulating the zigzag. Furthermore, we obtain a reduction in the compressive stress spike to $\sim 1/4$ the simulated value for a sharp edge. However, the zigzag does not completely eliminate the presence of the spike. We also mention that the $\sigma_{x'z}$ torsion stress, when present during high-temperature processing, is known to enhance dislocation formation in silicon near a stripe edge.[20] Since our study shows the stresses resulting from diamond stripe growth are thermal, we rule out the formation of dense dislocations at high temperature as a potential stress-relaxation mechanism in silicon beneath the diamond stripe edge.

In summary, we report a bottom-up approach for selective CVD growth of polycrystalline diamond on silicon substrates. Well-defined stripes are demonstrated with widths as small as $\sim 20\,\mu$m. UV micro-Raman maps are employed to investigate stress throughout the diamond and in the silicon immediately beneath the stripes. Measurements are well-described using simulated thermal stress distributions across the diamond stripes with various widths. Both simulation and experimental results indicate that compressive stress on CVD diamond reaches a maximum value in the center of the stripe and relaxes at the edges. Stress in the silicon interface region is the highest at the diamond stripe edge. Far from the diamond stripes, the stress in silicon is relaxed.

Funding for this work was provided by the Army Research Office (W911NF-15-1-0424) under the direction of Dr. Joe Qui.

[1]M. Kuc, M. Wasiak, and R. P. Sarzala, IEEE Trans. Compon., Packag., Manuf. Technol. **5**(4), 474–482 (2015).
[2]Y. Han, B. L. Lau, G. Y. Tang, and X. W. Zhang, IEEE Trans. Compon., Packag., Manuf. Technol. **5**(12), 1740–1746 (2015).
[3]J. Blevins, G. D. Via, K. Chabak, A. Bar-Cohen, J. J. Maurer, and A. Kane, in *Proceedings of CS MANTECH Conference* (May 2014), 105–108.
[4]Q. Z. Wu, Y. H. Xu, J. J. Zhou, Y. C. Kong, T. S. Chen, Y. Wang, F. J. Lin, Y. Fu, Y. H. Jia, X. D. Zhao, B. Yan, and R. M. Xu, ECS J. Solid State Sci. Technol. **6**(12), Q171–Q178 (2017).
[5]B. L. Hancock, M. Nazari, J. Anderson, E. Piner, F. Faili, S. Oh, D. Twitchen, S. Graham, and M. Holtz, Appl. Phys. Lett. **108**, 211901 (2016).
[6]C. Y. Hua, X. B. Yan, J. J. Wei, J. C. Guo, J. L. Liu, L. X. Chen, L. F. Hei, and C. M. Li, Diamond Related Mater. **73**, 62–66 (2017).
[7]M. J. Edwards, C. R. Bowen, D. W. E. Allsopp, and A. C. E. Dent, J. Phys. D: Appl. Phys. **43**, 385502 (2010).
[8]V. Jirasek, T. Izak, M. Varga, O. Babchenko, and A. Kromka, Thin Solid Films **589**, 857–863 (2015).
[9]A. Masood, M. Aslam, M. A. Tamor, and T. J. Potter, J. Electrochem. Soc. **138**(11), L67–L68 (1991).
[10]S. Prawer and R. J. Nemanich, Philos. Trans. R. Soc. London, Ser. A: Math. Phys. Eng. Sci. **362**(1824), 2537–2565 (2004).
[11]H. Windischmann and K. J. Gray, Diamond Related Mater. **4**(5-6), 837–842 (1995).
[12]I. De Wolf, Semicond. Sci. Technol. **11**(2), 139 (1996).
[13]M. Nazari, B. L. Hancock, J. Anderson, A. Savage, E. L. Piner, S. Graham, F. Faili, S. Oh, D. Francis, D. Twitchen, and M. Holtz, Appl. Phys. Lett. **108**(3), 031901 (2016).
[14]M. Holtz, J. C. Carty, and W. M. Duncan, Appl. Phys. Lett. **74**, 2008–2010 (1999).
[15]K. A. Christensen and M. D. Morris, Appl. Spectrosc. **52**(9), 1145–1147 (1998).
[16]Y. Okada and Y. Tokumaru, J. Appl. Phys. **56**(2), 314–320 (1984).
[17]G. A. Slack and S. F. Bartram, J. Appl. Phys. **46**(1), 89–98 (1975).
[18]P. Hess, J. Appl. Phys. **111**(5), 051101 (2012).
[19]M. A. Hopcroft, W. D. Nix, and T. W. Kenny, J. Microelectromech. Syst. **19**(2), 229–238 (2010).
[20]S. M. Hu, J. Appl. Phys. **50**(7), 4661–4666 (1979).
[21]D. E. Aspnes and A. A. Studna, Phys. Rev. B **27**(2), 985–1009 (1983).
[22]E. Anastassakis, A. Pinczuk, E. Burstein, F. H. Pollak, and M. Cardona, Solid State Commun. **8**(2), 133 (1970).
[23]I. DeWolf, H. E. Maes, and S. K. Jones, J. Appl. Phys. **79**(9), 7148–7156 (1996).